J. Fluid Mech. (2009), *vol.* 625, *pp.* 353–370. © 2009 Cambridge University Press
doi:10.1017/S0022112008005703 Printed in the United Kingdom

Modelling carbon dioxide sequestration in layered strata

JEROME A. NEUFELD[1]† AND HERBERT E. HUPPERT[1]

[1]Institute of Theoretical Geophysics, Department of Applied Mathematics and Theoretical Physics, University of Cambridge, CMS Wilberforce Road, Cambridge CB3 0WA, UK

(Received 6 August 2008 and in revised form 15 December 2008)

Motivated by the geological sequestration of carbon dioxide (CO_2), we study the propagation of gravity currents in a porous medium bounded by a thin layer of much lower permeability. We formulate a model for drainage assuming that the fluid remains simply connected throughout. Using this model we examine the propagation of both two-dimensional and axisymmetric currents numerically. We find that for the fixed-flux situation solutions approach a steady state which is described analytically. The approach to this final solution depends on both the permeability contrast and thickness of the thin layer, and in many cases the current first overshoots before relaxing back to its ultimate steady state. Finally, we examine propagation along multiple thin, lower permeability layers as a reduced-order model of the plume of CO_2 currently being injected at Sleipner in the North Sea.

1. Introduction

Global energy consumption has roughly doubled from 1970 to 2005 and shows no sign of abating (Rogner *et al.* 2007). Approximately 80 % of this consumption comes from the combustion of fossil fuels, resulting in current anthropogenic emissions of approximately 27 gigatonnes per year of carbon dioxide (CO_2). Emissions on such a large scale have led to an increase in the atmospheric concentration of CO_2 from 280 parts per million (p.p.m.) in 1950 to 379 p.p.m. in 2005, likely responsible for the concomitant increase in the average global temperature. While several strategies have been proposed for both short- and long-term mitigation of anthopogenic emissions, carbon capture and storage (CCS) promises to be one of the dominant mechanisms for easing the transition from an energy infrastructure built around the combustion of fossil fuels to a more carbon-neutral scheme. Storage of CO_2 is potentially an attractive solution and may take place by pumping supercritical (liquid-like) CO_2 into large, porous geological formations which exist beneath many continents and under the oceans. The largest industrial-scale example of such a scheme has been operated by Statoil and partners at Sleipner in the North Sea, where approximately 1 million tonnes of CO_2 have been sequestered each year since 1996. Other such experiments are either ongoing or planned in Algeria, Australia, Canada, China and the United States.

Experiments of this scope and scale motivate both fundamental investigations and a deeper understanding of the dynamics involved as fluids propagate through complex porous media, and this understanding in turn underlies estimates of the long-term

† Email address for correspondence: j.neufeld@damtp.cam.ac.uk

https://doi.org/10.1017/S0022112008005703 Published online by Cambridge University Press

viability of sequestered CO_2. In the case of the Sleipner field, supercritical CO_2 is injected near the base of the Utsira sand formation and, due to its relative density, rises as a buoyant plume through the approximately 200 metre thick formation before it is ultimately stopped by the Nordland shale, a relatively impermeable cap rock at the top of the formation. The rise of this CO_2 has been imaged seismically in 1999, 2001 and 2002 (together with a pre-injection survey in 1994), and recent analyses by Arts *et al.* (2004) and Bickle *et al.* (2007) show that the rise of the CO_2 plume is greatly affected by nine intervening, low-permeability mudstone layers of typical thickness 1 metre and with maximum thickness of 5 metres. They showed that as the buoyant CO_2 plume impinges on these layers it spreads out as a gravity current, before ultimately leaking through either a series of discrete fractures in the thin, low-permeability shale layers or as a diffuse, buoyancy-driven flux through these layers. By neglecting any leakage through these thin shale layers, Bickle *et al.* (2007) analysed the spreading, using the similarity solutions of Lyle *et al.* (2005). This analysis clearly showed the controlling influence of the shale layers in directing the buoyant propagation of the CO_2 plume and provided valuable constraints on the physical properties of the Utsira formation which govern fluid flow.

The injection of CO_2 into a heterogeneous reservoir saturated in brine is a rich and complex problem. At the typical temperatures and pressures encountered in saline aquifers CO_2 is a supercritical fluid which is immiscible with the ambient brine. In addition, depending on the specific conditions the CO_2 may be 5–40 times less viscous than the interstitial brine (Nordbotten, Celia & Bachu 2005), leading to a highly convoluted interface, or multiphase region, separating the two pure fluids. Models incorporating both the viscosity contrast and the multiphase region have been proposed by Nordbotten & Celia (2006) and Hesse, Orr, & Tchelepi (2008) respectively, and each model illustrates the critical importance of the large density contrast between CO_2 and the interstitial brine in the dynamics of injection. In what follows, we neglect the complex dynamics of the multiphase region, focusing solely on the role of buoyancy on propagation in heterogeneous media in an effort to capture the leading-order behaviour of such currents.

The buoyant propagation of fluids within porous media of uniform permeability has been studied previously by a number of authors. The axisymmetric propagation of a current along an impermeable barrier has been studied by Lyle *et al.* (2005), who found a series of similarity solutions describing these flows. In particular, they found that for currents driven by a constant flux of fluid the radius of the current spreads like the square root of time since the initiation of injection, a result which compares extremely well with their experiments in that geometry. Further work by Vella & Huppert (2006) investigated the influence of a sloping cap rock on the propagation as a function of the angle of inclination and showed that at early times these currents propagate axisymmetrically before transitioning to a regime in which the downslope nose spreads linearly with time. These results may be useful in interpreting data from the Otway project in Australia (Berly, Sharma & Cook 2008) in which up to 100 000 tonnes of CO_2 are to be injected in 2008/2009 into a layer (the Waarre C formation) which slopes at about 5°.

The influence of drainage on the spreading of low-Reynolds-number gravity currents in air has been investigated by a series of authors. Acton, Huppert & Worster (2001) examined the case of low-Reynolds-number gravity currents propagating over a deep porous medium. They formulated, and experimentally verified, a simple drainage law which incorporates both the hydrostatic pressure associated with the overlying current and the weight of the interstitial fluid. Models incorporating this drainage

https://doi.org/10.1017/S0022112008005703 Published online by Cambridge University Press

law well characterized a series of fixed-volume experiments. This drainage model was subsequently used by Pritchard & Hogg (2002) to investigate the propagation of two-dimensional gravity currents within porous media over a deep, lower permeability layer. Finally, Spannuth *et al.* (2009) has compared the predictions of axisymmetric propagation and drainage with the flow of a viscous fluid over a range of porous media.

Similar work on the propagation of a gravity current within a porous medium which drains through a thin, lower permeability layer has been conducted by Pritchard, Woods & Hogg (2001). Their model assumes that once fluid penetrates through the low-permeability layer it is immediately removed from the system in a presumably convective manner. Thus, drainage from the current is driven solely by the weight of the overlying current. We consider the alternate limit here, where fluid remains simply connected as it drains through the low-permeability layer, giving rise to the possibility that this drained fluid can affect subsequent flows. In all likelihood, draining fluid will undergo a Rayleigh–Taylor instability leading to a flux of fluid through the lower permeability layer the nature of which is complicated by the effects of both permeability heterogeneity and the contact between immiscible fluids of differing viscosity. Our approach therefore constitutes an upper bound on the effect the drained fluid may have on the subsequent evolution of the gravity current.

The present paper focuses on gravity currents which propagate within a uniform porous medium over a thin layer of much lower permeability (an imperfect seal). The effect of drainage through this low-permeability layer on the propagation of a gravity current provides a model by which we analyse currents spreading in multi-layered strata. We begin in § 2 by formulating a drainage law, assuming that the fluid remains simply connected throughout. This drainage law is then used to study currents propagating over thin, low-permeability layers in two dimensions. In § 3 we extend the model and examine axisymmetric flows. These models are then used to examine geometries comparable to those found in the North Sea at the Sleipner carbon-sequestration site in § 4. We use the axisymmetric results to examine the propagation of buoyant CO_2 through multiple low-permeability layers. Finally, we summarize the work and its relevance to CO_2 sequestration in § 5.

2. Propagation over a thin, low-permeability layer: two-dimensional geometry

2.1. *Geometry*

We commence by considering the evolution of a gravity current within a uniform porous medium of permeability k interleaved by a thin layer of much lower permeability $k_b < k$ $(0 > z > -b)$ as shown in figure 1. A gravity current of height $z = h(x, t) > 0$ propagates under the action of gravity along the thin, low-permeability layer, driven by a relatively small density difference $\Delta\rho$ with the ambient interstitial fluid, and subsequently drains through this thin layer. We note that while for experimental convenience we consider the case of a dense intruding current propagating over a thin, low-permeability layer, the model constructed describes equally well the propagation of a light intruding current at the base of a low-permeability layer in the Bousinesq limit $\Delta\rho/\rho \ll 1$, where ρ is the density of the ambient interstitial fluid. Finally, to examine the dynamics of propagation and drainage we restrict our attention to the case of uniform viscosity μ but note that differences between the viscosity of the injected and ambient fluids may play a key role in the dynamics of a spreading CO_2 plume (Nordbotten *et al.* 2005; Thompson & Huppert 2009).

https://doi.org/10.1017/S0022112008005703 Published online by Cambridge University Press

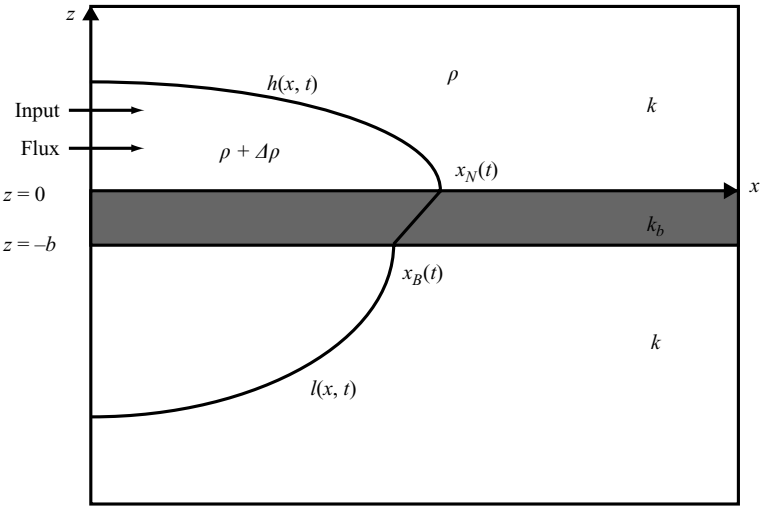


FIGURE 1. Schematic illustration of the propagation of a fluid of density $\rho + \Delta\rho$ over a low-permeability layer of width b and permeability k_b. The interface between the injected fluid and the interstitial fluid is given by $h(x,t)$ and the draining current by $l(x,t)$. The radial extent of the current in the upper layer is given by $x_N(t)$ and in the lower layer by $x_B(t)$.

2.2. *Drainage*

After an initial transient, such currents are typically much larger in their lateral extent than they are in their depth. In such a circumstance motion within the overriding current is predominantly horizontal, and so pressure can be assumed to be nearly hydrostatic within the overriding current:

$$p = \rho g'(h - z), \tag{2.1}$$

where $g' = g\Delta\rho/\rho$ is the reduced gravity and $h(x,t)$ varies as a function of the distance from the injection point x and the time since initiation t. We fix our vertical coordinate z to the top of the low-permeability layer (occupying the region $-b < z < 0$). Flow within both the underlying low-permeability layer and the lower high-permeability layer is predominantly vertical and is driven by both the hydrostatic head of the overriding current and the weight of the draining current as expressed by the vertical component of Darcy's law

$$\frac{\partial p_i}{\partial z} = -\rho g' - \frac{\mu}{k_i} w_i, \tag{2.2}$$

where p_i, k_i and w_i are the pressure, permeability and vertical velocity of layer i. If we assume that this draining region remains simply connected, then pressure within the lower two layers can be expressed as

$$p_2 = \rho g' \left\{ h\left(1 + \frac{z}{b}\right) - \frac{(l-b)z}{b}\left[\frac{h + (1-\Lambda)b}{l - (1-\Lambda)b}\right]\right\} \tag{2.3}$$

and

$$p_3 = \rho g'(l + z)\left[\frac{h + (1-\Lambda)b}{l - (1-\Lambda)b}\right], \tag{2.4}$$

where $\Lambda = k/k_b$ is the ratio of permeabilities; $l(x,t)$ is the depth to which the fluid has drained; and the subscripts 2 and 3 refer to regions $-b < z < 0$ and $z < -b$

https://doi.org/10.1017/S0022112008005703 Published online by Cambridge University Press

respectively. Note that this solution follows from continuity of both pressure and vertical fluxes at $z=-b$. The resulting drainage velocity at $z=0$ is given by

$$w(x,0,t)=\begin{cases}-\dfrac{k_b g'}{\nu}\left[1+\dfrac{h}{l}\right], & l<b,\\[2ex] -\dfrac{kg'}{\nu}\left[\dfrac{h+l}{(\Lambda-1)b+l}\right], & l\geqslant b.\end{cases} \tag{2.5}$$

The evolution equation governing the height of the current, and the depth to which it penetrates, is given by

$$\phi\frac{\partial h}{\partial t}-\frac{kg'}{\nu}\frac{\partial}{\partial x}\left(h\frac{\partial h}{\partial x}\right)=w(x,0,t) \tag{2.6}$$

and

$$-\phi\frac{\partial l}{\partial t}=w(x,0,t), \tag{2.7}$$

following Acton *et al.* (2001) and Pritchard *et al.* (2001). Here ϕ is the porosity of the matrix which, for simplicity, we have taken as equal in all three regions. Following many previous authors (Huppert 1982; Acton *et al.* 2001; Lyle *et al.* 2005, for example) we consider the case of a current whose volume increases as qt^{α} for constants q and α. However, instead of tracking this volume in both the advancing current and the drainage front, we impose a flux at the origin. Therefore we write the boundary conditions on the system as

$$\left[\frac{kg'}{\nu}h\frac{\partial h}{\partial x}\right]_0=-\alpha q t^{\alpha-1}, \tag{2.8}$$

$$\left[\frac{kg'}{\nu}h\frac{\partial h}{\partial x}\right]_{x_N}=0, \tag{2.9}$$

$$h(x_N(t),t)=0 \tag{2.10}$$

and

$$l(x_B(t),t)=b, \tag{2.11}$$

where (2.8) defines the flux at the origin; (2.9) requires zero flux through the nose of the current; and (2.10) and (2.11) respectively define the nose of the current $x_N(t)$ and the point at which drainage passes through the bottom of the low-permeability layer $x_B(t)$. We note further that the boundary conditions (2.8) and (2.9) are related to a global statement of conservation of mass,

$$\int_0^{x_N}\phi h\,\mathrm{d}x-\int_0^t\int_0^{x_N}w(x,0,t)\,\mathrm{d}x\,\mathrm{d}t=qt^{\alpha}, \tag{2.12}$$

through both temporal and spatial integrals of (2.6).

2.3. *Scaling*

The governing equations can be made non-dimensional through the introduction of the dimensionless variables

$$H=h/S_V,\quad L=l/S_V,\quad B=b/S_V,\quad X=x/S_H\quad\text{and}\quad T=t/S_T, \tag{2.13a,b,c,d,e}$$

where the horizontal, vertical and temporal scales are given by

$$S_H=S_V=(q/\phi\gamma^{\alpha})^{1/(2-\alpha)}\quad\text{and}\quad S_T=(q/\phi\gamma^{2})^{1/(2-\alpha)} \tag{2.14a,b,c}$$

https://doi.org/10.1017/S0022112008005703 Published online by Cambridge University Press

respectively, and $\gamma = kg'/(\phi\nu)$ is the settling velocity within the porous medium. Finally, we note that the vertical velocity scales with the settling velocity γ.

The non-dimensional evolution equations governing the height and depth of the current then become

$$\frac{\partial H}{\partial T} - \frac{\partial}{\partial X}\left(H\frac{\partial H}{\partial X}\right) = W(X, 0, T) \tag{2.15}$$

and

$$-\frac{\partial L}{\partial T} = W(X, 0, T), \tag{2.16}$$

where the drainage velocity is given by

$$W(X, 0, T) \equiv \begin{cases} -\dfrac{H+L}{\Lambda L} & L < B, \\ -\dfrac{H+L}{\Upsilon + L} & L \geqslant B. \end{cases} \tag{2.17}$$

Here we see that the current initially begins to drain through the low-permeability layer with the drainage velocity proposed by Acton *et al.* (2001). However, once the fluid penetrates through the low-permeability layer the form of the drainage law is modified by the additional parameter

$$\Upsilon \equiv (\Lambda - 1)B, \tag{2.18}$$

which is the product of the non-dimensional permeability contrast and the non-dimensional thickness of the low-permeability layer. It is this parameter which plays the dominant role in determining the evolution of the current.

Equation (2.15) is subject to the non-dimensional boundary conditions

$$\left[H\frac{\partial H}{\partial X}\right]_0 = -\alpha T^{\alpha-1}, \tag{2.19}$$

$$\left[H\frac{\partial H}{\partial X}\right]_{X_N} = 0, \tag{2.20}$$

where again

$$H(X_N(T), T) = 0, \tag{2.21}$$

$$L(X_B(T), T) = -B \tag{2.22}$$

define the nose and lateral extent of drainage into the lowermost layer respectively.

The draining current admits a steady state solution, irrespective of Υ, for $\alpha = 1$. In the limit $T \to \infty$, where $L \gg H$ and $L \gg \Upsilon$,

$$\frac{\partial}{\partial X}\left(H\frac{\partial H}{\partial X}\right) = 1. \tag{2.23}$$

Integration thus yields the steady state extent and profile, which are

$$X_N = 1 \quad \text{and} \quad H(X, T) = X_N - X, \tag{2.24a, b}$$

respectively. We note that this steady state extent and profile, which we have arrived at through the long-time consideration of drainage modelled by (2.17), is similar to the steady state profile found by Pritchard *et al.* (2001), using a fixed vertical drainage.

https://doi.org/10.1017/S0022112008005703 Published online by Cambridge University Press

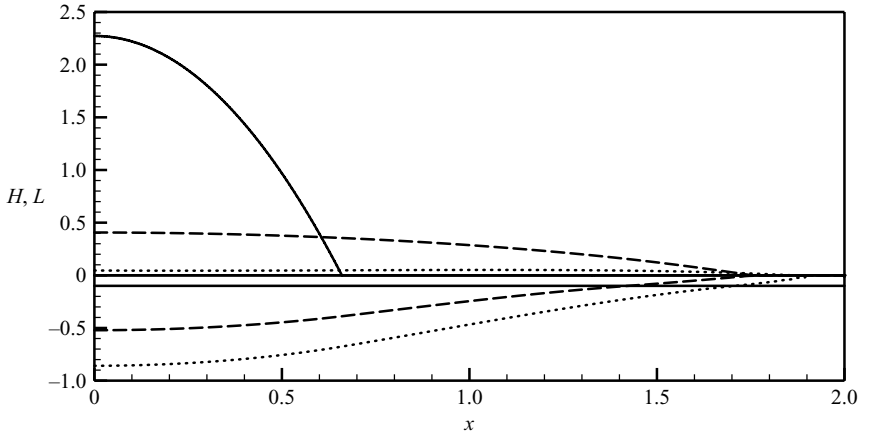


FIGURE 2. Profiles of a two-dimensional gravity current of fixed volume release ($\alpha = 0$) for $B = 0.1$ and $\Upsilon = 2$ ($\Lambda = 21$). The current profiles are shown for $T = 0.03$ (solid line), 1.0 (dashed line) and 2.0 (dotted line).

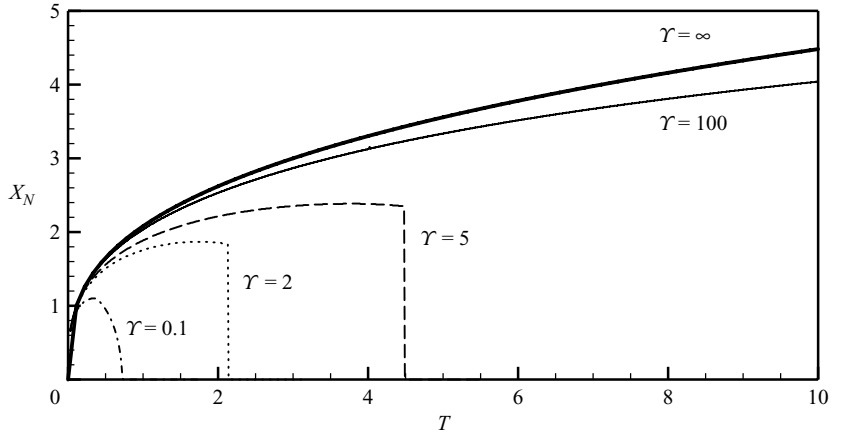


FIGURE 3. The extent of a two-dimensional porous gravity current of fixed volume ($\alpha = 0$) is plotted as a function of time in the limit of no drainage (similarity solution, bold solid line), for $\Upsilon = 100$ (solid line), $\Upsilon = 5$ (dashed line), $\Upsilon = 2$ (dotted line) and $\Upsilon = 0.1$ (dashed–dotted line).

2.4. *Constant volume:* $\alpha = 0$

The model described by (2.15) and (2.16) was solved numerically on a fixed grid $X = [0, 10]$ with $N = 1501$ points, using an implicit Crank–Nicholson scheme centred in time and space (see Press *et al.* 1997). A predictor–corrector iteration was used, first assessing the nonlinear diffusivity at the original time step and subsequently at the half time step. The results were tested against the solutions of Pattle (1959) and Lyle *et al.* (2005) and were found to be in excellent agreement.

Numerical solutions showing profiles of the the two-dimensional spreading of a fixed volume of fluid for $\Upsilon = 2$ are shown in figure 2, and the extent as a function of time are shown for a variety of Υ in figure 3. In each case the propagation is initiated at time $T_0 = 0$ with $H = L = 0$. The current subsequently evolves through several distinct regimes, each characterized by a differing mode of drainage.

https://doi.org/10.1017/S0022112008005703 Published online by Cambridge University Press

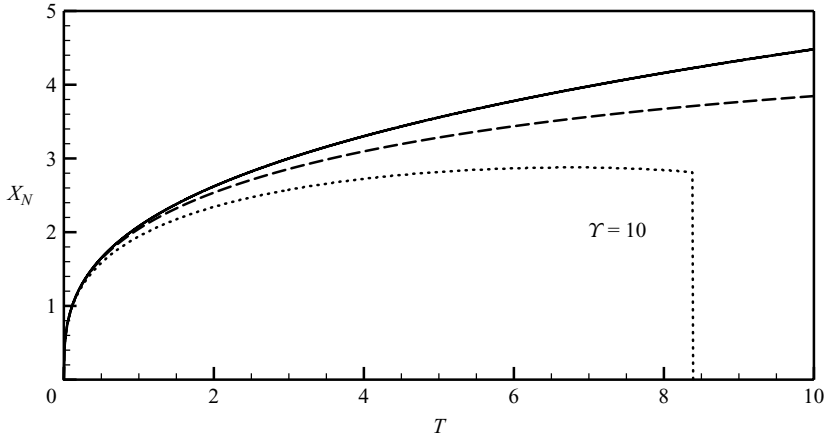


FIGURE 4. Comparison of the extent of a porous gravity current of fixed volume ($\alpha = 0$) in the limit of no drainage given by the similarity solution (solid line), the model of Pritchard *et al.* (2001) (dashed line) and the present analysis for which $\Upsilon = 10$ (dotted line).

At early times when $H \gg L$ and especially for $\Upsilon \gg 1$ there is little drainage. The current is essentially non-draining, in which case it is well approximated by the similarity solution first described by Pattle (1959). In this limit the height of the current is described by

$$H(X, T) = \frac{1}{6} T^{-1/3} \left(9^{2/3} - \frac{X^2}{T^{2/3}} \right), \tag{2.25}$$

and its extent evolves as

$$X_N(T) = 9^{1/3} T^{1/3}. \tag{2.26}$$

This similarity solution represents an upper bound on both the height and extent of the current for all Υ, as is clearly seen in figure 3.

At intermediate times, for which $H > L$, limited drainage becomes important to the propagation of the current. For $\Upsilon \gg 1$ the solution of Pritchard *et al.* (2001) is recovered. Their work, which modelled the propagation of a fixed volume current over a low-permeability layer, resulted in the evolution equation

$$\frac{\partial H}{\partial T} - \frac{\partial}{\partial X} \left(H \frac{\partial H}{\partial X} \right) = -\frac{H}{\Upsilon} \tag{2.27}$$

((2.14) in their work) for the height of the current but neglected enhanced drainage due to the presence of the bottom high-permeabiltiy layer. They found an analytic expression for the extent of the current given by

$$X_N(T) = \left[9\Upsilon \left(1 - \mathrm{e}^{-T/\Upsilon} \right) \right]^{1/3}, \tag{2.28}$$

which is compared to both the similarity solution and our numerical solution for $\Upsilon = 10$ in figure 4. At early times, when drainage is driven primarily by the weight of the overriding current, the agreement between the two models is quite favourable. However, at later times the drainage becomes dominated by the weight of the fluid in the lower layer, thus increasing the drainage through the low-permeability layer. This slows the advance of the front.

For large values of Υ the current drains completely once it has reached this maximum extent as indicted in both figure 2 and figure 3, whereas for small Υ

https://doi.org/10.1017/S0022112008005703 Published online by Cambridge University Press

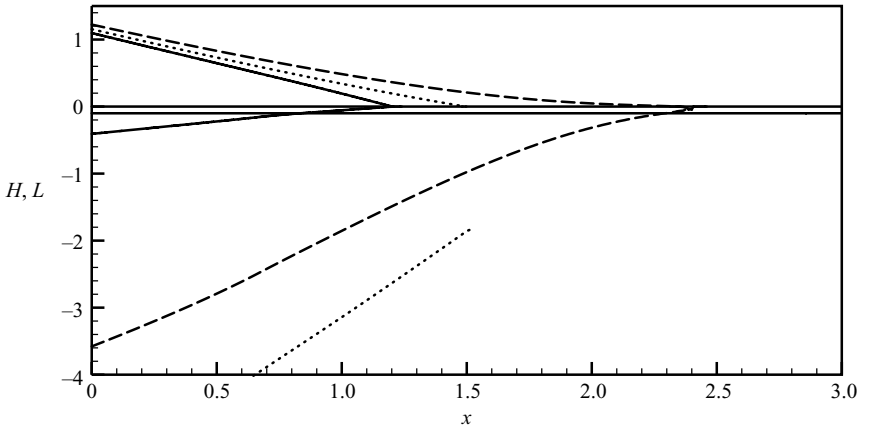


FIGURE 5. Profiles of a two-dimensional porous gravity current with fixed flux at the origin ($\alpha = 1$) and in which $B = 0.1$ and $\Upsilon = 2$ ($\Lambda = 21$). Current profiles are shown for $T = 1.0$ (solid line), 5.0 (dashed line) and 7.0 (dotted line). Note that only the portion of the draining fluid affecting the propagation of the overriding current has been plotted for clarity.

the current continuously recedes to the origin. The limit of $\Upsilon \to 0$ has been studied previously by Pritchard & Hogg (2002) for fixed-volume currents. Their results show a similar pattern of propagation followed by recession of the current driven by drainage.

2.5. *Fixed flux*: $\alpha = 1$

The spreading of a current from a source with fixed flux is shown in figure 5 for a variety of Υ. The behaviour for fixed flux is more varied than that for the fixed-volume case, with propagation showing at least three distinct regimes. At early times, before drainage has become fully established, the current first propagates at the rate given by the non-draining similarity solution

$$X_N(T) = \eta_N T^{2/3}, \tag{2.29}$$

where $\eta_N \simeq 1.48$ is obtained through integration of the similarity function found in Huppert & Woods (1995) for $\alpha = 1$. As is the case for fixed-volume release, this similarity solution provides a bound on the maximal extent of the current and is recovered in the limit $\Upsilon \to \infty$. Once drainage is established, but while $H > L$, the current rapidly extends to a value in excess of its ultimate steady state extent for $\Upsilon > 1$. Then as the depth of penetration $L \gg H$ the current gradually relaxes back to its steady state extent of $X_N = 1$ as predicted by (2.24*a*). Example profiles for the intermediate value $\Upsilon = 2$ are shown in figure 5 in which, for clarity, only the portion of the drained fluid still actively contributing to the propagation of the gravity current has been plotted. The resultant evolution of the extent of the current is then plotted in figure 6 for a variety of Υ. It is important to note that, while the depth of drainage monotonically increases with time, the height of the gravity current and hence its maximum lateral extent depend sensitively on the form of the drainage. These quantities therefore reflect the increasing importance of drainage through a succession of regimes, leading to an ultimate steady state.

https://doi.org/10.1017/S0022112008005703 Published online by Cambridge University Press

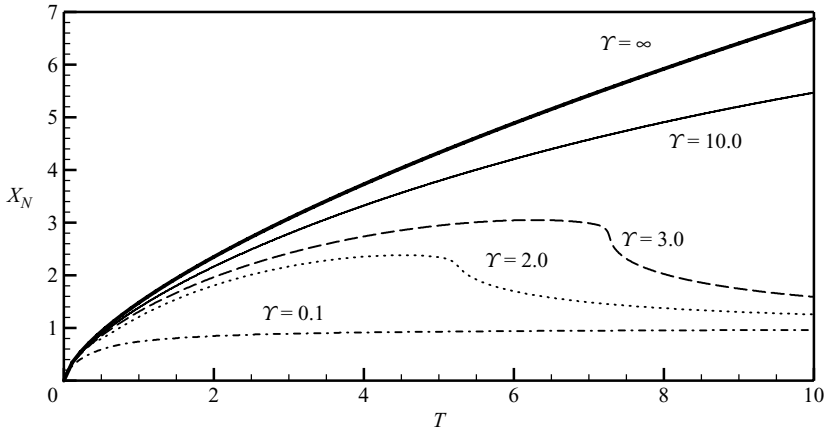


FIGURE 6. The extent of a two-dimensional porous gravity current of fixed flux ($\alpha = 1$) is plotted as a function of time in the limit of no drainage (similarity solution, bold solid line), for $\Upsilon = 10$ (solid line), $\Upsilon = 3$ (dashed line), $\Upsilon = 2$ (dotted line) and $\Upsilon = 0.1$ (dashed–dotted line). For all finite values of Υ the curves approach the steady state limit $X_N = 1$ as $T \to \infty$.

3. Propagation over a thin, low-permeability layer: axisymmetric geometry

A similar analysis can be made for the spread of an axisymmetric current over a thin, low-permeablity layer. Using the same model of drainage, we find the equations governing height and depth of penetration are

$$\phi \frac{\partial h}{\partial t} - \frac{kg'}{\nu} \frac{1}{r} \frac{\partial}{\partial r} \left(rh \frac{\partial h}{\partial r} \right) = w(r, 0, t) \tag{3.1}$$

and

$$-\phi \frac{\partial l}{\partial t} = w(r, 0, t), \tag{3.2}$$

where $w(r, 0, t)$ is given by (2.5). Equations (3.1) and (3.2) are subject to the boundary conditions

$$\lim_{r \to 0} \left[2\pi r \frac{kg'}{\nu} h \frac{\partial h}{\partial r} \right] = -\alpha q t^{\alpha - 1}, \tag{3.3}$$

$$\left[2\pi r h \frac{\partial h}{\partial r} \right]_{r_N} = 0, \tag{3.4}$$

$$h(r_N(t), t) = 0 \tag{3.5}$$

and

$$l(r_B(t), t) = b, \tag{3.6}$$

which again constrain the flux at the origin, require zero flux through the nose of the current and define both the nose of the current and the furthest point at which the draining current enters the lowermost layer.

3.1. *Axisymmetric scalings*

The vertical, radial and temporal scales are given by

$$S_V = S_R = (q/\phi\gamma^{\alpha})^{1/(3-\alpha)} \quad \text{and} \quad S_T = (q/\phi\gamma^3)^{1/(3-\alpha)} \tag{3.7a, b, c}$$

https://doi.org/10.1017/S0022112008005703 Published online by Cambridge University Press

respectively, where again $\gamma = kg'/(\phi\nu)$. Application of these scalings yields the non-dimensional governing equations

$$\frac{\partial H}{\partial T} - \frac{1}{R}\frac{\partial}{\partial R}\left(RH\frac{\partial H}{\partial R}\right) = W(R, 0, T) \tag{3.8}$$

and

$$-\frac{\partial L}{\partial T} = W(R, 0, T), \tag{3.9}$$

with the non-dimensional boundary conditions

$$\lim_{R\to 0}\left[2\pi RH\frac{\partial H}{\partial R}\right] = -\alpha T^{\alpha-1}, \tag{3.10}$$

$$\left[2\pi RH\frac{\partial H}{\partial R}\right]_{R_N} = 0, \tag{3.11}$$

$$H(R_N(T), T) = 0 \tag{3.12}$$

and

$$L(R_B(T), T) = 0. \tag{3.13}$$

The long-time evolution of the fixed flux ($\alpha = 1$) spreading axisymmetric current can be evaluated in a manner identical to the two-dimensional case. In the limit $T \to \infty$ we find that both $L \gg H$ and $L \gg \Upsilon$, so

$$\frac{1}{R}\frac{\partial}{\partial R}\left(RH\frac{\partial H}{\partial R}\right) = 1. \tag{3.14}$$

Integration with boundary conditions (3.10)–(3.12) therefore yields the steady state radius and current profile, which are

$$R_N = \pi^{-1/2} \quad \text{and} \quad H(R, T\to\infty) = \sqrt{\frac{1}{2}\left(R^2 - R_N^2\right) - R_N^2\log(R/R_N)}, \tag{3.15a, b}$$

respectively. This steady state position and profile are similar to the steady state solutions found by Pritchard *et al.* (2001), using a fixed vertical drainage.

3.2. *Axisymmetric propagation*

Both the constant-volume and fixed-flux cases display a behaviour similar to that found in two dimensions. For constant volume, profiles (figure 7) and plots of the radial extent (figure 8) show that currents ultimately drain completely into the underlying low-permeability layer. For fixed flux ($\alpha = 1$) the same transition from a drainage velocity dominated by the hydrostatic pressure of overriding fluid to a velocity dominated by the weight of the draining fluid is seen. Here profiles (figure 9) and plots of the radial extent of the current (figure 10) show the initial extension of the current followed by a retreat to the same analytical steady state radius $R_N = \pi^{-1/2}$ independent of Υ.

4. Multiple layers: CO_2 sequestration at the Sleipner field

CO_2 has been sequestered on an industrial scale at the Sleipner field in the North Sea since 1996. Seismic images analysed by Arts *et al.* (2004) and Bickle *et al.* (2007) clearly show that the dynamics of the plume propagation within this 200 metre thick sand formation is dominated by a series of nine thin, low-permeability shale layers.

https://doi.org/10.1017/S0022112008005703 Published online by Cambridge University Press

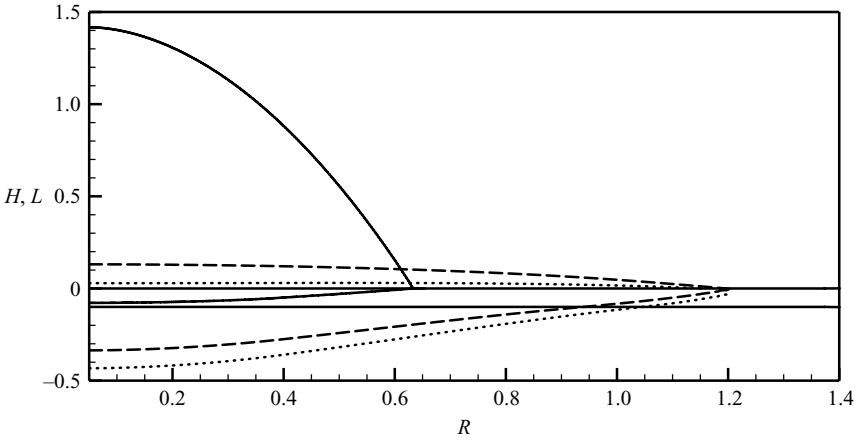


FIGURE 7. Profiles of a fixed volume ($\alpha = 0$) axisymmetric porous gravity current propagating over a thin, low-permeability layer with $B = 0.1$ and $\Upsilon = 2$ ($\Lambda = 21$). Current profiles are shown for $T = 0.04$ (solid line), 1.0 (dashed line) and 1.5 (dotted line).

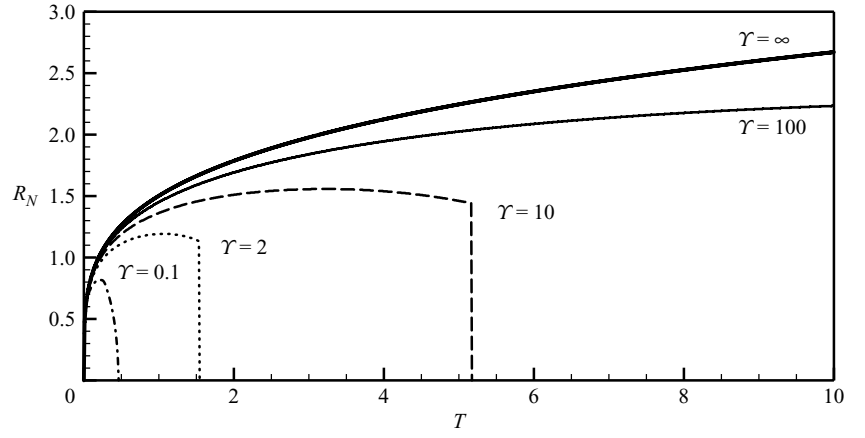


FIGURE 8. The radial extent of a fixed volume ($\alpha = 0$) axisymmetric porous gravity current is plotted as a function of time in the limit of no drainage (similarity solution, bold solid line), for $\Upsilon = 100$ (solid line), $\Upsilon = 10$ (dashed line), $\Upsilon = 2$ (dotted line) and $\Upsilon = 0.1$ (dashed–dotted line).

These layers, which are typically one meter thick, spread the buoyant plume laterally. To date, seismic images remain inconclusive as to whether vertical flow within the formation is dominated by leakage through these layers or through a series of high-permeability fractures. Here we examine the limit of uniform leakage driven by both the hydrostatic pressure of the underlying CO_2 and the fluid which has penetrated through these layers.

We build our model of this multi-layered system, using the results of § 3 in which we have examined the propagation of a gravity current along a single low-permeability layer. In our multi-layered model, propagation at each layer is analysed separately. The buoyant rise of CO_2 within the formation is initiated with a constant flux of fluid beneath the first layer (layer 0). The propagation along each subsequent layer

https://doi.org/10.1017/S0022112008005703 Published online by Cambridge University Press

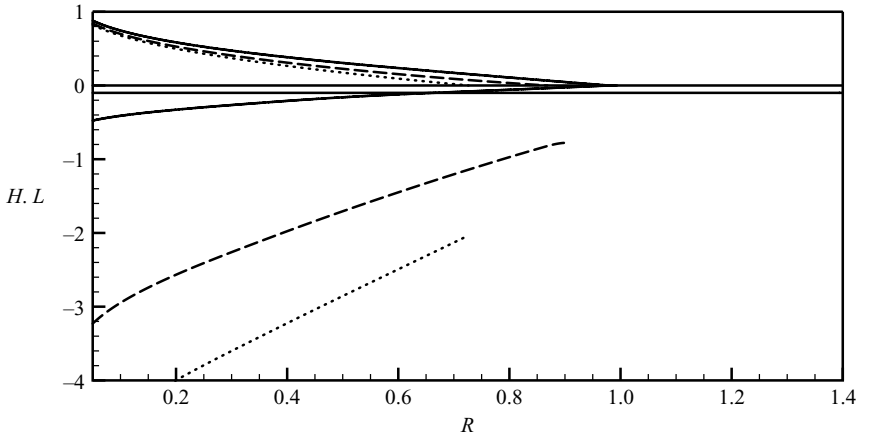


FIGURE 9. Profiles of a fixed flux ($\alpha = 1$) axisymmetric porous gravity current propagating over a thin, low-permeability layer with $B = 0.1$ and ($\Upsilon = 2$) $\Lambda = 21$. Current profiles are shown for $T = 1$ (solid line), 5 (dashed line) and 7 (dotted line). Note that only the portion of the draining fluid effecting the propagation of the overriding current has been plotted for clarity.

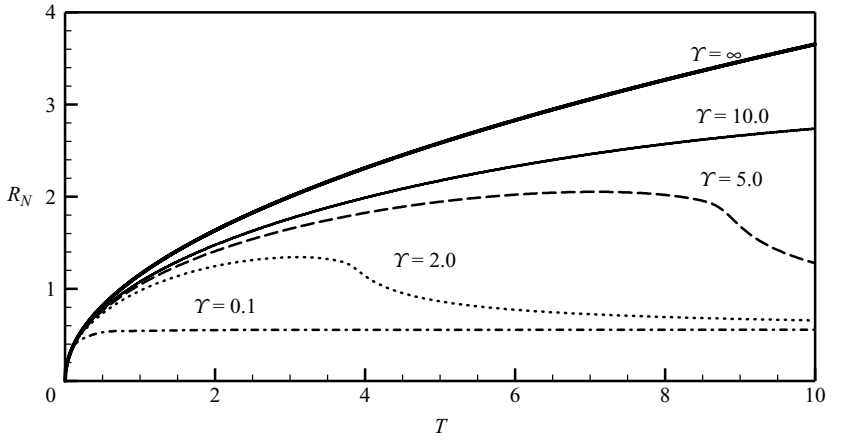


FIGURE 10. The radial extent of a fixed flux ($\alpha = 1$) axisymmetric gravity current is plotted as a function of time in the limit of no drainage (similarity solution, bold solid line), for $\Upsilon = 10$ (solid line), $\Upsilon = 5$ (dashed line), $\Upsilon = 2$ (dotted line) and $\Upsilon = 0.1$ (dashed–dotted line). All values for finite Υ approach the steady state limit $R_N = \pi^{-1/2}$ as $T \to \infty$.

is then driven by the integrated flux draining through the preceding layer as pictured in figure 11.

The results of the model are presented in figure 12 which show a series of snapshots in time of the buoyant plume as it rises through the formation. Flow in each layer is driven by the flux through the preceding layer and in turn provides a flux into subsequent layers as shown in figure 13. The ultimate radial extent at each layer is plotted as a function of time in figure 14. The picture which develops is of the rise of a plume whose head broadens through interaction with each subsequent layer as shown schematically in figure 15. However, as found in the model of a single low-permeability layer, the radial extent at any given layer ultimately returns to the scaled value $R_N = \pi^{-1/2}$. In a typical reservoir geometry such as that found at Sleipner, the

https://doi.org/10.1017/S0022112008005703 Published online by Cambridge University Press

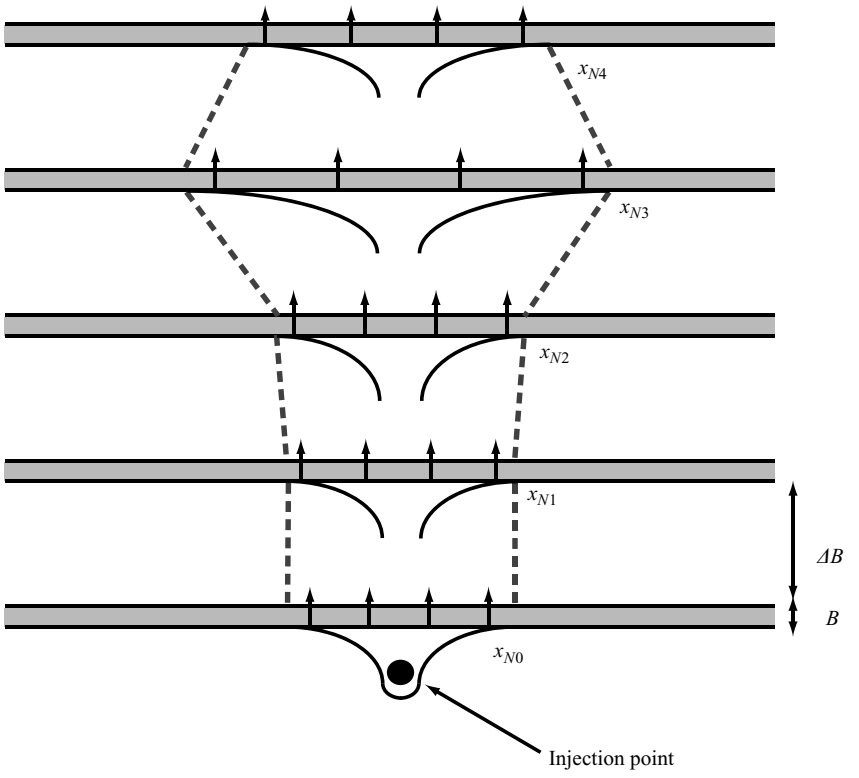


FIGURE 11. Schematic illustration of a CO_2 plume rising in a reservoir with multiple layers. A constant flux of buoyant fluid is injected beneath the first horizon under which it spreads axisymmetrically and through which it drains. The spatially integrated drainage through each layer is then input as a time-dependent flux into the subsequent layer. At each layer the spread of the buoyant CO_2 is illustrated by the solid line, while the vertical dashed line indicates the lateral extent of the plume.

behaviour of the rising plume illustrated in figure 15 is replicated throughout all N layers until an impermeable cap rock is reached. At much longer times, propagation along this cap rock may more closely resemble the similarity solution presented by Lyle *et al.* (2005) with deviations due to the vertical permeability structure of the form given by Anderson, McLaughlin & Miller (2003).

The value of such simplified models of buoyant propagation within complex reservoir geometries is in their ability to predict universal behaviour from which reservoir properties can be assessed. In the present model the key components are the separation distance between subsequent layers ΔB, the thickness of each layer and permeability contrast with the bulk reservoir as expressed by the parameter Υ, the source flux q and the bulk drainage velocity γ.

5. Discussion and conclusion

The propagation and drainage of gravity currents through, and into, porous media are motivated by a host of environmental and geophysical problems. An understanding of such currents may play a key role in determining the long-term fate of sequestered CO_2. Here, motivated by seismic observations of buoyant supercritical CO_2 upwelling from the injection point at the Sleipner field, we have studied

https://doi.org/10.1017/S0022112008005703 Published online by Cambridge University Press

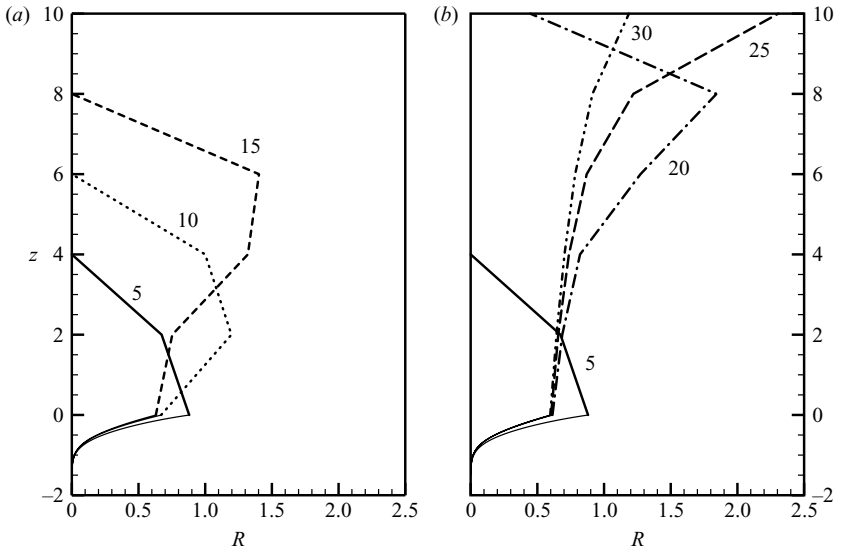


FIGURE 12. The outer envelope of a buoyant CO_2 plume rising in a multi-layered porous medium plotted for times $T = 5$ (solid line), 10 (dotted line), 15 (short-dashed line), 20 (dash–dotted line), 25 (long-dashed line) and 30 (dashed–dotted–dotted line). Low permeability layers are located at $z = 0, 2, 4, 6, 8$ and 10, with parameters $B = 0.1$ and $\Upsilon = 2$ ($\Lambda = 21$) and layer separation $\Delta B = 2$. At the early times shown in (a) the plume impinges on each layer and spreads dramatically. At the later times shown in (b), the lateral extent of the plume decreases as drainage due to upwelling material increases, ultimately asymptoting to its steady state extent.

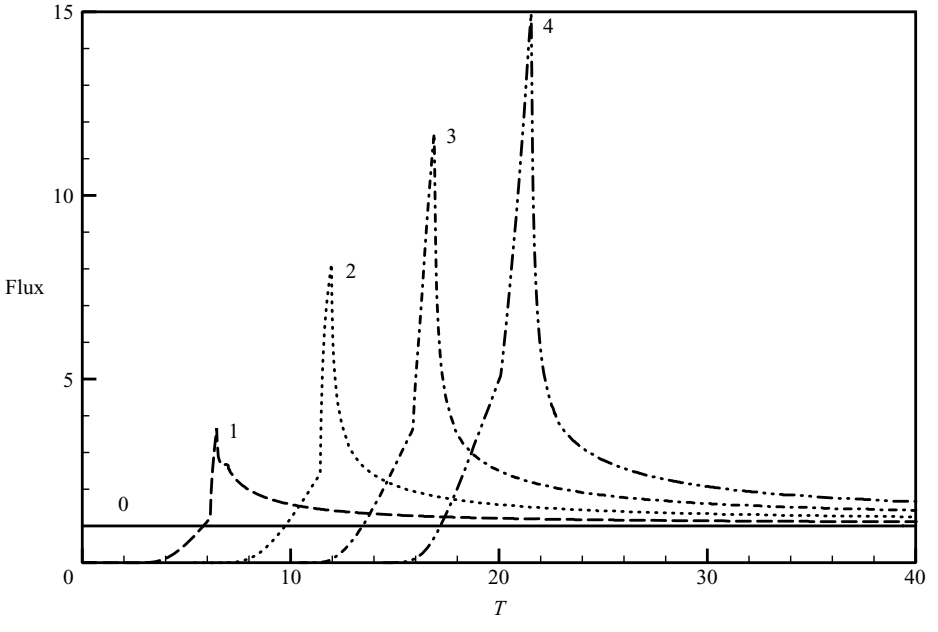


FIGURE 13. The non-dimensional flux is plotted as a function of time into layer 0 (solid line), layer 1 (dashed line), layer 2 (dotted line), layer 3 (dashed–dotted line) and layer 4 (dashed–dotted–dotted line). Parameter values are $B = 0.1$ and $\Upsilon = 2$ ($\Lambda = 21$) with layer separation $\Delta B = 2$. Note that the flux into the original layer (layer 0) is held fixed with time, with non-dimensional value 1.

https://doi.org/10.1017/S0022112008005703 Published online by Cambridge University Press

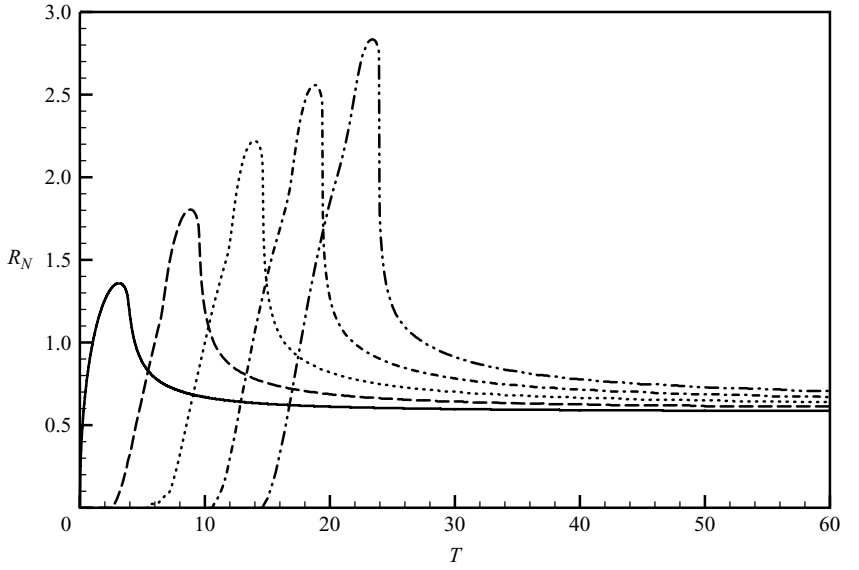


FIGURE 14. Radial extent as a function of time of a buoyant plume spreading at a series of low-permeability layers characterized by $B = 0.1$ and $\Upsilon = 2$ ($\Lambda = 21$) and with vertical spacing $\Delta B = 2$.

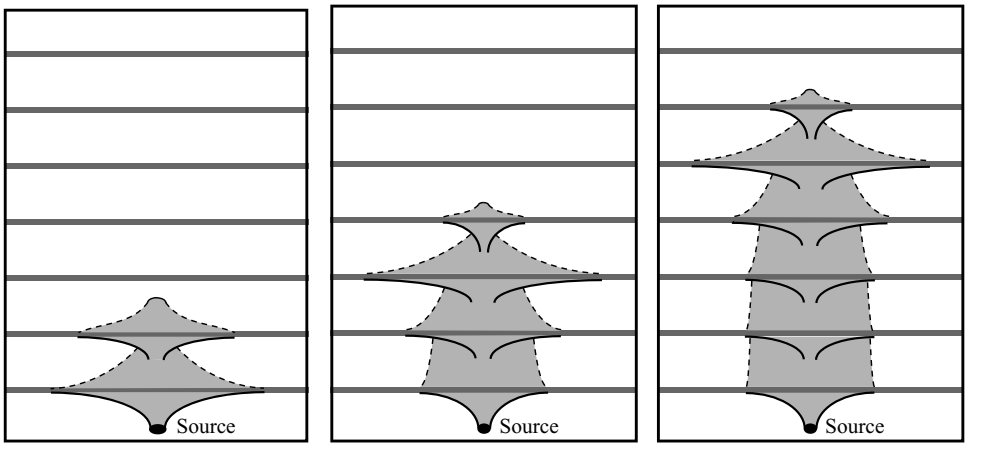


FIGURE 15. An illustration showing the propagation of a CO_2 plume through a reservoir composed of layered strata. We note that the plume has maximum lateral extent at the head, while width of the tail is given by the analytic steady state.

the propagation of such currents along thin, low-permeability layers in both two-dimensional and axisymmetric geometries. The propagation of porous gravity currents across thin layers of much lower permeability has been previously examined assuming that fluid plays no role in drainage once it passes through the low-permeability layer. However, in the limit in which the fluid remains simply connected we find that propagation can occur in three distinct regimes. First, fluid propagates over the low-permeability layer, and drainage is driven primarily by the weight of the overlying fluid. This mode of drainage leads to rapid extension of the current. Subsequently, as the thickness of the draining fluid exceeds the depth of the low-permeability

https://doi.org/10.1017/S0022112008005703 Published online by Cambridge University Press

layer, the weight of the drained fluid contributes to the drainage velocity, thereby halting further propagation of the gravity current. Finally, as the weight of the underlying fluid dominates drainage we find that the extent of both two-dimensional and axisymmetric currents recedes to a steady state value, which we have determined analytically.

This model for propagation along single thin, low-permeability layers has been extended to examine flow within layered strata, motivated by the industrial-scale CO_2 project at Sleipner in the North Sea. Propagation of the buoyant CO_2 takes place as a plume whose head broadens and thins as it progresses towards the top of the formation before it ultimately recedes to the analytically determined steady state. We find that propagation can be characterized by only a few key parameters defining the input flux, the thickness and vertical separation of the thin layers and the permeability contrast between the thin, low-permeability layers and the host formation. This reduction in the number of reservoir parameters needed to predict the behaviour of such a buoyant plume is important given the dearth of quantitative measurements of key rock properties such as the permeabilities and the uncertainty in seismic reconstructions of the geological structure.

Finally, the present study provides the basis for addressing the role of viscosity differences between CO_2 and the ambient fluid, residual trapping of the injected CO_2 and flow in tilted formations (such as those seen at the Otway project in Australia) on the propagation of injected CO_2 through layered strata. This study also highlights the importance of future work constraining the form of drainage through layered media, particularly in the presence of large viscosity contrasts, surface tension and lateral heterogeneity in structures of low-permeability layers in the form of fractures.

We are grateful for insightful comments by Peter Cook, Jonathan Ennis-King, Mark Hallworth, Andrew Hogg, Lincoln Patterson and David Pritchard on an earlier version of this paper. The research of H. E. H. is partially supported by the Royal Society Wolfson Merit Award.

REFERENCES

Acton, J. M., Huppert, H. E. & Worster, M. G. 2001 Two-dimensional viscous gravity currents flowing over a deep porous medium. *J. Fluid Mech.* **440**, 359–380.

Anderson, D. M., McLaughlin, R. M. & Miller, C. T. 2003 The averaging of gravity currents in porous media. *Phys. Fluids* **15** (10), 2810–2829.

Arts, R., Eiken, O., Chadwick, A., Zweigel, P., van der Meer, L. & Zinszner, B. 2004 Monitoring of CO_2 injected at Sleipner using time-lapse seismic data. *Energy* **29**, 1383–1392.

Berly, T., Sharma, S. & Cook, P. 2008 CO_2CRC Otway project: regulatory challenges and lessons learned. *APPEA J.* **48**.

Bickle, M., Chadwick, A., Huppert, H. E., Hallworth, M. & Lyle, S. 2007 Modelling carbon dioxide accumulation at Sleipner: implications for underground carbon storage. *Earth Planet. Sci. Lett.* **255**, 164–176.

Hesse, M. A., Orr, Jr, F. M. & Tchelepi, H. A. 2008 Gravity currents with residual trapping. *J. Fluid Mech.* **611**, 35–60.

Huppert, H. E. 1982 The propagation of two-dimensional and axisymmetric viscous gravity currents over a rigid horizontal surface. *J. Fluid Mech.* **121**, 43–58.

Huppert, H. E. & Woods, A. W. 1995 Gravity-driven flows in porous layers. *J. Fluid Mech.* **292**, 55–69.

Lyle, S., Huppert, H. E., Hallworth, M., Bickle, M. & Chadwick, A. 2005 Axisymmetric gravity currents in a porous medium. *J. Fluid Mech.* **543**, 293–302.

Nordbotten, J. M. & Celia, M. A. 2006 Similarity solutions for fluid injection into confined aquifers. *J. Fluid Mech.* **561**, 307–327.

https://doi.org/10.1017/S0022112008005703 Published online by Cambridge University Press

Nordbotten, J. M., Celia, M. A. & Bachu, S. 2005 Injection and storage of CO_2 in deep saline aquifers: analytical solution for CO_2 plume evolution during injection. *Transport Porous Med.* **58**, 339–360.

Pattle, R. E. 1959 Diffusion from an instantaneous point source with a concentration-dependent coefficient. *Quart. J. Mech. Appl. Math.* **12** (4), 407–409.

Press, W. H., Teukolsky, S. A., Vetterling, W. T. & Flannery, B. P. 1997 *Numerical Recipes in Fortran 77: The Art of Scientific Computing*, 2nd ed. Cambridge University Press.

Pritchard, D. & Hogg, A. J. 2002 Draining viscous gravity currents in a vertical fracture. *J. Fluid Mech.* **459**, 207–216.

Pritchard, D., Woods, A. W. & Hogg, A. J. 2001 On the slow draining of a gravity current moving through a layered permeable medium. *J. Fluid Mech.* **444**, 23–47.

Rogner, H. H., Zhou, D., Bradley, R., Crabbé, P., Edenhofer, O., Hare, B., Kuijpers, L. & Yamaguchi, M. 2007 *Climate Change 2007: Mitigation. Contribution of Working Group III to the Fourth Assessment Report of the Intergovernmental Panel on Climate Change*. Cambridge University Press.

Spannuth, M. J., Neufeld, J. A., Wettlaufer, J. S. & Worster, M. G. 2009 Axisymmetric viscous gravity currents flowing over a porous medium. *J. Fluid Mech.* **622**, 135–144.

Thompson, E. L. & Huppert, H. E. 2009 Carbon dioxide sequestration in aquifers: effects of viscosity. *J. Fluid Mech.* (in prep).

Vella, D. & Huppert, H. E. 2006 Gravity currents in a porous medium at an inclined plane. *J. Fluid Mech.* **555**, 353–362.

https://doi.org/10.1017/S0022112008005703 Published online by Cambridge University Press